A Dual-CP Multibeam Transmit-Array Antenna Based on Anisotropic Impedance Surfaces and Hybrid Phase Compensation

Xuanfeng Tong, Zhi Hao Jiang, Hao Chen, Fan Wu, Jingyang Cao, Ronan Sauleau, Wei Hong

A Dual-CP Multi-Beam Transmit-Array Antenna Based on Anisotropic Impedance Surfaces and Hybrid Phase Compensation

Xuanfeng Tong, *Student Member*, *IEEE*, Zhi Hao Jiang, *Member*, *IEEE*, Hao Chen, Fan Wu, *Member*, *IEEE*, Jingyang Cao, Ronan Sauleau, *Fellow*, *IEEE*, and Wei Hong, *Fellow*, *IEEE*

***Abstract*—In this paper, a dual-circularly-polarized (dual-CP) multi-beam transmit-array (TA) antenna is proposed and demonstrated based on anisotropic impedance surfaces (AISs) and hybrid phase compensation strategy. A set of eight fully-planarized TA cells based on cascaded AISs are designed with a constant dynamic phase difference between each other, possessing a periodicity of $0.48\lambda_0 \times 0.48\lambda_0$ and a total thickness of $0.71\lambda_0$, where λ_0 is the free-space wavelength at center frequency. By introducing Berry phase determined rotation angles on the eight designed cells, dual-CP transmissive phase delays can be achieved independently. Moreover, planar dual-CP antenna arrays are designed and utilized as the feed cluster of the multi-beam TA. The bifocal dual-CP multi-beam TA antenna generates eight RHCP beams and eight LHCP beams. The measured peak gain values are between 21.1 and 23.7 dBic, while the AR values are all below 3 dB for all the beams.**

***Index Terms*—Anisotropic impedance surface (AIS), dual-circularly-polarization, millimeter-wave, multi-beam, transmit-arrays.**

I. INTRODUCTION

CURVED dielectric lenses and metallic reflectors based on accumulated-phase determined by optical path length difference are commonly used conventional solutions for achieving high-gain radiated beams [1], [2]. Recently, their planarized counterparts, namely, transmit-arrays (TAs) and reflect-arrays (RAs) have gathered a great amount of attention due to the absence of shortcomings such as bulky size and curved structures [3], [4]. In addition, antennas possessing circularly-polarized (CP) radiation properties are amenable due to the reduction of sensitivity to the relative orientation between the transmitting and receiving devices. Hence, CP TAs have been widely investigated due to their advantages of having no feed blockage and being less sensitive to surface distortion as compared with RAs.

In contrast to single-CP TAs [5]–[9], dual-CP TAs with independent control of polarization have gained recently increased attention due to their ability for increased channel capacity and function multiplexing [10], [11]. In [10], a dual-functional-layer dual-CP TA is proposed by combing the dual-LP TA on the bottom and an LP-to-CP polarizer on the top, which possesses a 1-dB gain bandwidth of 7.6% with an AR of 2.9 dB at 29 GHz. A single-functional-layer dual-CP TA enabled by hybrid phase compensation techniques and antenna-filter-antenna (AFA) cells is reported in [11]. It achieves a measured bandwidth of 12% within which both the gain variation and AR are smaller than 2 dB for the final TA. However, the reported dual-CP TAs own the disadvantages of significant panel thickness [10] and insertion loss [10], [11]; they also suffer from complex fabrication constraints due to the existence of a large number of metallic vias [10], [11].

On the other hand, multi-beam antennas are promising for a number of applications since they can provide an expanded beam coverage, thus increasing the number of streams and enhance the spectral efficiency [12]. Multi-beam TAs based on a cluster of feed radiators have been demonstrated recently [13]–[17]. Comparing to single-CP/dual-LP multi-beam antennas [13]–[17], the dual-CP multi-beam antennas would hold a great promise for a number of applications ranging from space to wireless communications.

In this paper, the design and experimental verification of a dual-CP multi-beam TA integrated with planar dual-CP feeds is reported. Multi-layered AISs cells, hybrid phase compensation strategies, and a cluster of planar feed radiators are synthetically employed to achieve the TA antenna with diverse beam polarizations, independent beam directions, and 2-D beam coverage. The paper is organized as follows. Section II presents the design, modeling, and scattering parameters of the dual-CP TA cells. Section III reports the design and experiments of the planar dual-CP feed arrays as well as the bifocal dual-CP multi-beam TA antenna. Finally, conclusions are drawn in Section IV.

Manuscript received Oct. 10th, 2022. This work was supported in part by National Natural Science Foundation of China (NSFC) under Grants 62122019, 62293492, and 61901106, in part by the China Mobile Communication Co., Ltd. Research Institute, and in part by The Major Key Project of PCL (PCL2021A01-2). (*Corresponding author: Zhi Hao Jiang*)

X. Tong, H. Chen, and F. Wu are with the State Key Laboratory of Millimeter Waves, School of Information Science and Engineering, Southeast University, Nanjing 210096, China.

Z. H. Jiang and W. Hong are with the State Key Laboratory of Millimeter Waves, School of Information Science and Engineering, Southeast University, Nanjing 210096, China, and also with the Purple Mountain Laboratories, Nanjing 211111, China (e-mail: zhihao.jiang@seu.edu.cn).

J. Cao is with Institute of Wireless and Terminal Technology, China Mobile Communication Co., Ltd. Research Institute, Beijing 100053, China.

R. Sauleau is with Univ Rennes, 1CNRS, IETR - UMR 6164, F-35000 Rennes, France.

This article has been accepted for publication in IEEE Antennas and Wireless Propagation Letters. This is the author's version which has not been fully edited and content may change prior to final publication. Citation information: DOI 10.1109/LAWP.2023.3234699

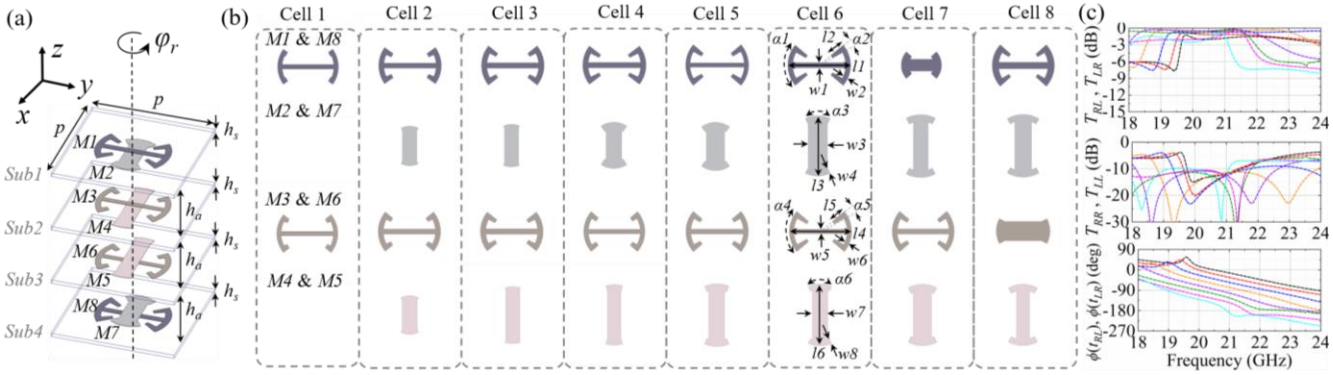

Fig. 2. (a) 3-D schematic of the proposed unit cell. The relative permittivity of the substrate is 3.55 with a loss tangent of 0.0027. (b) Top views of the metallic layers of all eight designed unit cells, where $\alpha 2 = 11°$ and $\alpha 5 = 11°$. (c) Simulated CP transmission magnitudes and cross-polarized CP transmission phases of the eight cells.

TABLE I DIMENSIONS OF THE METALLIC LAYERS OF THE EIGHT DESIGNED UNIT CELLS (UNITS: MM).

	M1 & M8					*M2 & M7*				*M3 & M6*					*M4 & M5*			
	w1	*l1*	*w2*	*l2*	*α1*	*w3*	*l3*	*w4*	*α3*	*w5*	*l4*	*w6*	*l5*	*α4*	*w7*	*l6*	*w8*	*α6*
Cell 1	0.3	4	0.3	0.37	70.9°	0	0	0	0°	0.29	4.1	0.29	0.52	77°	0	0	0	0°
Cell 2	0.34	4.16	0.34	0.71	71.4°	0.95	2.63	0.22	51.4°	0.34	4.17	0.34	0.67	78.3°	0.98	2.59	0.22	54.3°
Cell 3	0.35	4.11	0.35	0.8	78°	0.94	2.83	0.14	43.4°	0.35	4.18	0.35	0.83	76.6°	0.92	3.83	0.17	30.6°
Cell 4	0.35	4.19	0.35	0.96	75°	1.03	3.1	0.45	67°	0.3	4.1	0.3	0.65	81.4°	0.9	4.1	0.41	32°
Cell 5	0.28	4.16	0.28	0.89	80.9°	1.2	3.18	0.41	71°	0.32	4.15	0.32	0.79	80.2°	1.05	4.2	0.41	45.1°
Cell 6	0.33	4.17	0.33	1.08	80°	1.25	4	0.35	48°	0.3	4.2	0.3	1.05	80°	1	4.19	0.35	43.8°
Cell 7	0.8	2.7	0.49	0	83.1°	0.98	4.2	0.43	55°	0.33	4.15	0.33	0.84	80.9°	1.2	4.1	0.43	55.5°
Cell 8	0.42	4.14	0.42	0.95	84.3°	1.1	4.22	0.4	61°	1.27	3.59	0.42	0	55°	0.86	4.12	0.4	56°

II. DUAL-CP MULTI-BEAM TA ANTENNA CONFIGURATION AND DUAL-CP TA CELL DESIGNS

A. Configuration of the Dual-CP Multi-beam TA Antenna

The configuration of the dual-CP multi-beam TA antenna is presented in Fig. 1, which contains eight dual-CP feeds distributed beneath a planar bifocal dual-CP TA at positions around the two foci of the TA. Each dual-CP feed, comprised by a four-element sub-array, can excite RHCP and LHCP radiated waves with a moderate beamwidth, respectively. The TA, on the other hand, can offer independent wavefront transfer functions for CP waves with opposite handednesses.

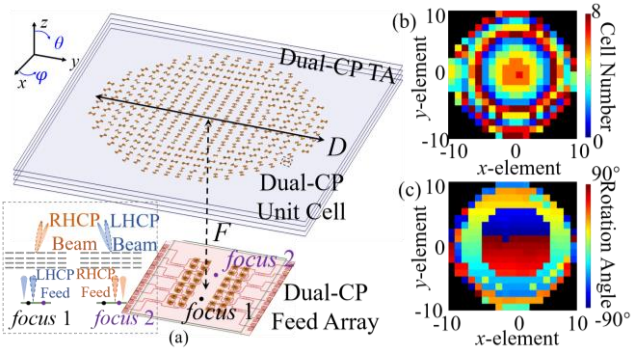

Fig. 1. (a) Configuration of the dual-CP multi-beam TA antenna. The inset shows the working principle of the bifocal dual-CP TA. Distributions of the (b) cell number and (c) cell rotation angle of the multi-beam TA across its radiating aperture.

B. Dual-CP TA Cells Based on Multi-layered AISs

For the purpose of modulating the dual-CP transmissive phase delay separately, hybrid phase compensation techniques, i.e., joint DP and BP compensations, need to be simultaneously introduced [11], [18]. Therefore, eight cells with a constant DP difference of 22.5°, i.e., a 4-bit resolution, are adopted for obtaining 3-bit dual-CP phase compensation. Each TA cell has four thin dielectric substrates made of Rogers 4003 with a thickness of h_s = 0.203 mm, which are separated by three air spacers each with a thickness of h_a = 3.2 mm [see Fig. 2(a)]. For each substrate, two layers of metallic patterns are placed on its top and bottom surfaces, respectively, which can be manufactured using low-cost well-controlled printed circuit board fabrication process. Therefore, the TA cells have a total of eight metallic layers denoted as *M1* ~ *M8* from top to bottom. All the unit cells possess a mirror symmetry with respect to the *x*-*y* plane [see Fig. 2(a)], with a periodicity of $p = 7$ mm ($\sim 0.48\lambda_0$) and a total thickness of 10.4 mm ($\sim 0.71\lambda_0$), where λ_0 is the free-space wavelength at 20.5 GHz.

For the purpose of designing well-performed unit cells, the metallic layers printed on both sides of the four substrates can be modeled as homogenized AISs characterized by diagonal surface admittance matrices of $\boldsymbol{Y_{sti}} = [Y_{stix}, 0; 0, Y_{stiy}]$ and $\boldsymbol{Y_{sbi}} = [Y_{sbix}, 0; 0, Y_{sbiy}]$ ($i = 1, 2, 3, 4$) [13], [19]. The eight AISs, which are divided into two groups, i.e., $\boldsymbol{Y}_{sb1}$, $\boldsymbol{Y}_{sb2}$, $\boldsymbol{Y}_{st3}$, $\boldsymbol{Y}_{st4}$ and $\boldsymbol{Y}_{st1}$, $\boldsymbol{Y}_{st2}$, $\boldsymbol{Y}_{sb3}$, $\boldsymbol{Y}_{sb4}$, are active under the *x*- and *y*-polarized wave excitation, respectively [see Fig. 3(a) and (b)]. The scattering parameters of the cells can be calculated by cascading the ABCD matrices of the AISs, four substrates, and three air layers. The distributions of the calculated transmission magnitudes and phases are reported in Fig. 3(c) and (d). According to the admittance values required for the cells as indicated by red and blue points in Fig. 3, eight specific cells are designed [see Fig. 2(b)] with their geometrical dimensions provided in Table. I.

The simulated CP scattering parameters of the designed TA cells are presented in Fig. 2(c) [20]. It can be seen that the averaged cross-polarized CP transmission magnitudes (T_{RL} and

T_{LR}) are larger than -2 dB, while the averaged co-polarized transmission magnitudes (T_{RR} and T_{LL}) are smaller than -11 dB in the frequency range from 19.5 to 21.75 GHz within which the cross-polarized CP transmission phases ($\phi(t_{RL})$ and $\phi(t_{LR})$) exhibit a linear phase change, indicating an operational bandwidth of about 11%. In order to provide true dual-CP transmissive phase compensation, the designed cells are rotated around their own geometrical centers for introducing additional BP delays. Consequently, the cross-polarized CP transmission phases can be independently controlled [see Fig. 4].

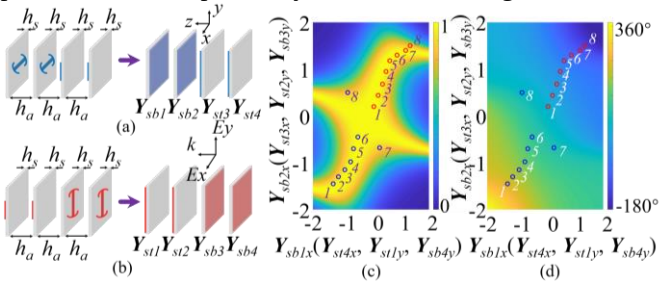

Fig. 3. Homogenized models of the unit cells for (a) *x*-polarization and (b) *y*-polarization. Analytically calculated transmission (c) magnitudes and (d) phases at normal incidence for *x*-polarization and *y*-polarization at 20.5 GHz.

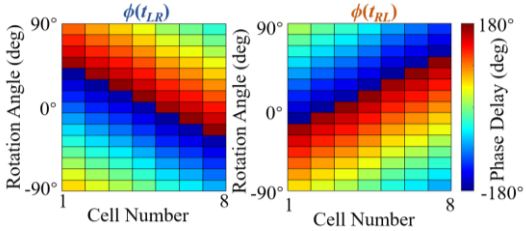

Fig. 4. Distributions of the simulated cross-polarized CP transmission phases at 20.5 GHz as a function of both cell number and cell rotation angle (φ_r).

III. Dual-CP Multi-Beam TA Antenna Demonstration

In most of the previously reported TAs, horn antennas are used as the feeds, resulting in an increased overall profile of the antenna [5]–[8], [10], [14], [17]. Alternatively, low-profile planar antennas with stable and symmetrical radiation patterns over a wide bandwidth have also been employed as the feeds for TAs [9], [11], [13], [15]–[16]. In this section, the design and experiments of planar dual-CP feed arrays and a dual-CP multi-beam TA antenna are presented.

A. Dual-CP Multi-beam TA Antenna Design

An amenable feed source should possess planar structures, wide impedance and AR bandwidth, and symmetrical radiation patterns with a moderate gain for balancing the profile and aperture efficiency of the TA antenna [3]. By cascading the feed network and the four-element array of dual-LP magnetoelectric (ME) dipoles, a dual-CP antenna is designed as the feeding source [see Fig. 5(a)] [21], which is fabricated and tested. The simulated and measured -10 dB beamwidths of the RHCP and LHCP beams are around 62° in both the *x*-*z* and *y*-*z* planes at 20.5 GHz [see Fig. 5(b)]. The simulated and measured gain and AR values as a function of frequency for the RHCP and LHCP waves are provided in Fig. 5(c) and (d). At frequencies from 19 to 22 GHz, the simulated and measured AR values are smaller than 2.5 dB, while the measured gain value fluctuates between 11.6 and 12.9 dBic for both RHCP and LHCP waves.

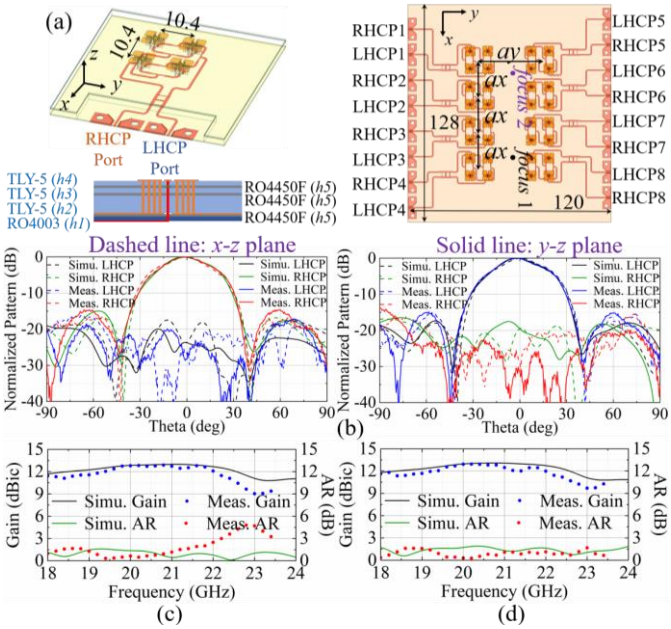

Fig. 5 (a) 3-D schematic of the dual-CP feed, and top view of the dual-CP feed array for the dual-CP multi-beam TA antenna, where *h1* = 0.203, *h2* = 1.52, *h3* = 0.13, *h4* = 0.25, *h5* = 0.1, *ax* = 21 mm, and *ay* = 36 mm. The relative permittivity and loss tangent values are 3.55 and 0.0027, 2.2 and 0.0009, 3.52 and 0.004 for Rogers 4003, TLY-5, Rogers 4450F, respectively. (b) Simulated and measured normalized CP radiation patterns in the *x*-*z* and *y*-*z* planes at 20.5 GHz. Simulated and measured gain and AR values as a function of frequency of the (c) RHCP and (d) LHCP beam.

Multi-beam TA antennas based on a cluster of dual-CP feeds can generate multiple spatially-interleaved dual-CP beams, with each beam corresponding to a specific feed [13], [22]. For generating 16 adjacent beams, eight planar dual-CP feeds in a 4 × 2 periodic arrangement are placed around the two foci of TA panel with their relative locations optimized [see Fig. 5(a)]. The multi-beam TA contains 308 cells with a diameter of 140 mm and a focal distance of 117 mm, corresponding to an *F*/*D* ratio of 0.84. The designed TA cells are arranged on the aperture for compensating the phase difference of the quasi-spherical waves emitted from the feeds and providing the phase gradients for beam deflection. Fig. 1(b) and (c) display the distributions of the cell number and cell rotation angle of the multi-beam TA.

For verifying the performance of the designed dual-CP multi-beam TA antenna, the TA panel together with the dual-CP feeds are simulated in HFSS. For simplicity, only four selected beams (Beam 1, Beam 5, Beam 12, and Beam 16) of the simulated 2-D normalized CP radiation patterns in their corresponding φ planes are presented in Fig. 6(c). The simulated beam directions of the produced beams agree well with the design targets. As it can be seen from Fig. 6(c) that the SLLs are all below -14 dB, while the cross-polarization levels are within an acceptable range of no more than -15 dB in the main beam region. In addition, for exhibiting the beam coverage area of the 16 produced beams, the simulated -3 dB contour patterns in the (*u*, *v*) space are reported in Fig. 6(b). For evaluating the gain variation and AR performance of the created 16 beams, the peak gain and AR values as a function of the beam number are displayed in Fig. 6(d). It shows that the simulated peak gain values vary between 21.8 and 24.2 dBic for all the beams at 20.5 GHz, while the AR values are all smaller than 3 dB.

This article has been accepted for publication in IEEE Antennas and Wireless Propagation Letters. This is the author's version which has not been fully edited and content may change prior to final publication. Citation information: DOI 10.1109/LAWP.2023.3234699

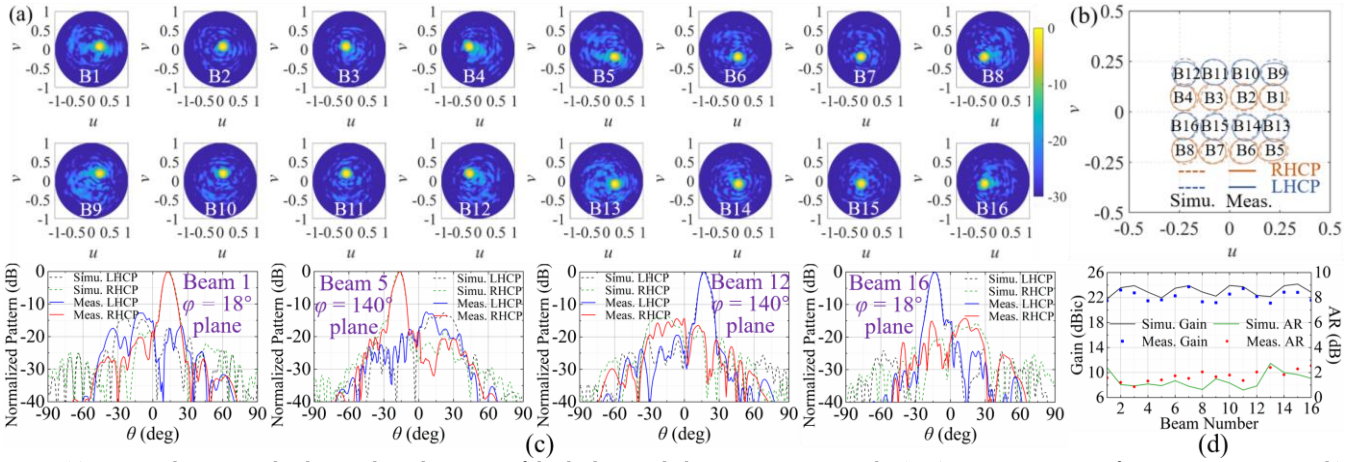

Fig. 6. (a) Measured 3-D normalized co-polarized patterns of the dual-CP multi-beam TA antenna in the (u, v) space at 20.5 GHz for Beam 1 – Beam 16. (b) Simulated and measured -3 dB contour patterns in the (u, v) space for the 16 produced beams of the dual-CP multibeam TA antenna at 20.5 GHz. (c) Simulated and measured normalized RHCP and LHCP patterns of the dual-CP multi-beam TA antenna in their corresponding φ planes for Beams 1, 5, 12, and 16 at 20.5 GHz. (d) Simulated and measured peak gain and AR values as a function of beam number of the dual-CP multibeam TA antenna at 20.5 GHz.

TABLE II A COMPARISON AMONG DIFFERENT MULTI-BEAM TA ANTENNAS

	Central Frequency	Polarization	Total Profile	F/D Ratio	Phase Compensation Technique	Peak Gain & Aperture Efficiency	3-dB Gain Bandwidth	Scanning Angle & Loss	Beam Coverage
[14]	10 GHz	Dual-LP	>7.3λ_0	0.72	DP	24.7 dBi / 23.5%	20.1%	20° / 2.2 dB	1-D
[15]	5.6 GHz	Dual-LP	5λ_0	0.5	DP	22.4 dBi / NA	13.8%	20° / 2.5 dB	1-D
[16]	5.5 GHz	Dual-LP	3.46λ_0	0.37	DP	20.9 dBi / 15.2%	NA	20° / 2.5 dB	1-D
[17]	30 GHz	Dual-LP	>15.2λ_0	1	DP	28.1 dBi / 40.9%	34.8%	20° / 3.2 dB	2-D
This Work	20.5 GHz	Dual-CP	8.8λ_0	0.84	DP + BP	23.7 dBic / 26%	19.9%	17° / 2.6 dB	2-D

B. *Experimental Results*

In order to verify the performance of the designed dual-CP multi-beam TA antenna, a prototype is fabricated, assembled, and experimentally characterized [see Fig. 7(a)]. The measured S-parameters of the dual-CP multi-beam TA antenna are shown in Fig. 7(b) and (c), without including the simulated results for simplicity. It can be seen that all the measured reflection coefficients are below -10 dB from 17 to 24 GHz. Besides, the mutual couplings from other ports to RHCP1 port and LHCP2 port are all below -15 dB between 17.8 and 22.4 GHz.

The radiation patterns are measured in a near-field chamber as shown in Fig. 7(a). The measured 3-D normalized co-polarized CP radiation patterns of Beam 1 – Beam 16 in the (u, v) space are provided in Fig. 6(a), where the weak cross-polarized patterns are not included here for succinctness. All the generated beams are pointed to the targeted directions [see Fig. 6(a)]. In addition, the measured 2-D normalized radiation patterns for Beam 1, Beam 5, Beam 12, and Beam 16 in their corresponding φ planes are presented in Fig. 6(c). The measured SLLs and cross-polarization levels are smaller than -15 dB. The measured -3 dB contour patterns are also shown in the Fig. 10(a). It can be seen that the measured results are consistent with the simulated ones. Moreover, the measured peak gain and AR values of Beam 1 – Beam 16 at 20.5 GHz are provided in Fig. 6(d). The measured gain variation and AR values are smaller than 3 dB for all the beams. In particular, the measured peak gain values are in the range of 21.1 – 23.7 dBic for all the beams at 20.5 GHz, indicating that the measured aperture efficiency varies between 14.3% and 26%. A comparison between the proposed integrated dual-CP multi-beam TA antenna and other multi-beam dual-polarized TA antennas is show Table II. It can be seen that the proposed TA antenna provides a 2-D beam coverage with orthogonal CP waves. Moreover, when comparing with other previously reported dual-polarized multi-beam TA antennas, it possesses a higher aperture efficiency benefiting from the smaller insertion loss of fully-planarized cells as well as the moderate gain and beamwidth of the designed dual-CP feeding sources.

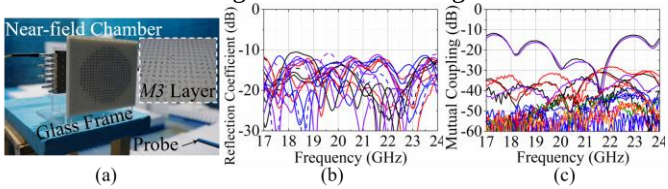

Fig. 7. (a) Photograph of the dual-CP multi-beam TA antenna. Measured (b) reflection coefficients for all the input ports and (c) mutual couplings from other ports to RHCP1 port and LHCP2 port of the multi-beam TA antenna.

IV. CONCLUSION

In summary, the design and experimental demonstration of the dual-CP multi-beam TA antenna is reported. The independent control of the transmission phases for orthogonal CP waves are achieved by employing the fully-planarized TA cells based on cascaded multi-layered AISs and BP determined rotation angles. Moreover, a planar dual-CP feed array is designed and intergated with the bifocal TA panel to generate 2-D beam coverage. The demonstrated dual-CP multi-beam TA antenna is a promising candidate for applications such as satellite communications, point-to-multipoint communications, and so on.

REFERENCE

[1] S. Rondineau, M. Himdi, and J. Sorieux, "A sliced spherical Luneburg lens," *IEEE Antennas Wireless Propag. Lett.*, vol. 2, pp. 163-166, 2003.

[2] S. K. Rao, "Parametric design and analysis of multiple-beam reflector antennas for satellite communications," *IEEE Antennas Propag. Mag.*, vol. 45, no. 4, pp. 26-34, Aug. 2003.

[3] J. Huang and J. A. Encinar, *Reflectarray Antennas*. New York, NY, USA: Wiley, 2008.

[4] A. H. Abdelrahman, F. Yang, A. Z. Elsherbeni, P. Nayeri, and C. A. Balanis, *Analysis and Design of Transmitarray Antennas*. San Francisco, CA, USA: Morgan & Claypool, 2017.

[5] L. Di Palma, A. Clemente, L. Dussopt, R. Sauleau, P. Potier, and P. Pouliguen, "Circularly polarized transmitarray with sequential rotation in Ka-band," *IEEE Trans. Antennas Propag.*, vol. 63, no. 11, pp. 5118-5124, Nov. 2015.

[6] C. Tian, Y. Jiao, and G. Zhao, "Circularly polarized transmitarray antenna using low-profile dual-linearly polarized elements," *IEEE Antennas Wireless Propag. Lett.*, vol. 16, pp. 465-468, 2017.

[7] F. Diaby, A. Clemente, K. T. Pham, R. Sauleau, and L. Dussopt, "Circularly polarized transmitarray antennas at Ka-Band," *IEEE Antennas Wireless Propag. Lett.*, vol. 17, no. 7, pp. 1204-1208, July 2018.

[8] Z. H. Jiang, L. Kang, T. Yue, W. Hong, and D. H. Werner, "Wideband transmit arrays based on anisotropic impedance surfaces for circularly polarized single-feed multibeam generation in the Q-band," *IEEE Trans. Antennas Propag.*, vol. 68, no. 1, pp. 217-229, Jan. 2020.

[9] J. Hu, H. Wong, and L. Ge, "A circularly-polarized multi-beam magneto-electric dipole transmitarray with linearly-polarized feeds for millimeter-wave applications," *IEEE Trans. Antennas Propag.*, vol. 70, no. 7, pp. 6012-6017, July 2022.

[10] K. T. Pham, A. Clemente, D. Blanco, and R. Sauleau, "Dual-circularly polarized high-gain transmitarray antennas at Ka-band," *IEEE Trans. Antennas Propag.*, vol. 68, no. 10, pp. 7223-7227, Oct. 2020.

[11] Z. H. Jiang, F. Wu, T. Yue, and W. Hong, "Wideband and low-profile integrated dual-circularly-polarized transmit-arrays enabled by antenna-filter-antenna phase shifting cells," *IEEE Trans. Antennas Propag.*, vol. 69, no. 11, pp. 7462-7475, Nov. 2021.

[12] W. Hong *et al*., "Multibeam antenna technologies for 5G wireless communications," *IEEE Trans. Antennas Propag.*, vol. 66, no. 12, pp. 6231–6249, Dec. 2017.

[13] Z. H. Jiang, Y. Zhang, J. Xu, Y. Yu, and W. Hong, "Integrated broadband circularly polarized multibeam antennas using Berry-phase transmit-arrays for Ka-band applications," *IEEE Trans. Antennas Propag.*, vol. 68, no. 2, pp. 859-872, Feb. 2020.

[14] K. Pham *et al*., "Design of wideband dual linearly polarized transmitarray antennas," *IEEE Trans. Antennas Propag.*, vol. 64, no. 5, pp. 2022-2026, May 2016.

[15] S. Li, Z. N. Chen, T. Li, F. H. Lin, and X. Yin, "Characterization of metasurface lens antenna for sub-6GHz dual-polarization full-dimension massive MIMO and multibeam dystems," *IEEE Trans. Antennas Propag.*, vol. 68, no. 3, pp. 1366-1377, Mar. 2020.

[16] Y. -H. Yu, Z. -Y. Zong, W. Wu, Q. Chen, and D. -G. Fang, "Dual-polarized linear array with overlapping handover of subarray to produce continuous beam scanning for transmitarray antenna," *IEEE Trans. Antennas Propag.*, vol. 69, no. 2, pp. 859-868, Feb. 2021.

[17] X. Wang, Y. Cheng, and Y. Dong, "Millimeter-wave dual-polarized metal transmitarray antenna with wide gain bandwidth," *IEEE Antennas Wireless Propag. Lett.*, vol. 21, no. 2, pp. 381-385, Feb. 2022.

[18] Z. H. Jiang, T. Yue, and W. Hong, "Low-profile and wideband dual-circularly polarized reflect-arrays based on rotated metal-backed dual-polarized aperture-coupled patch elements," *IEEE Trans. Antennas Propag.*, vol. 68, no. 3, pp. 2108-2117, Mar. 2020.

[19] Z. H. Jiang and W. Hong, "Design and experiments of bandwidth-controllable broadband monopole antennas with conformal anisotropic impedance surface coatings," *IEEE Trans. Antennas Propag.*, vol. 66, no. 3, pp. 1133-1142, March 2018.

[20] R. H. Phillion, and M. Okoniewski, "Lenses for circular polarization using planar arrays of rotated passive elements," *IEEE Trans. Antennas Propag.*, vol. 59, no. 4, pp. 1217-1227, April 2011.

[21] B. Feng, L. Li, K. L. Chung, and Y. Li, "Wideband widebeam dual circularly polarized magnetoelectric dipole antenna/array with meta-columns loading for 5G and beyond," *IEEE Trans. Antennas Propag.*, vol. 69, no. 1, pp. 219-228, Jan. 2021.

[22] Y. Hu, W. Hong, and Z. H. Jiang, "A multibeam folded reflectarray antenna with wide coverage and integrated primary sources for millimeter-wave massive MIMO applications," *IEEE Trans. Antennas Propag.*, vol. 66, no. 12, pp. 6875-6882, Dec. 2018.